External-Store Loads Using Nonplanar Lifting Surface Theory

William R. Chadwick*
U. S. Naval Weapons Laboratory, Dahlgren, Va.

Experimental data indicate clearly that pylon-induced loads are the largest contributor to the total aerodynamic side loads on externally mounted aircraft stores. Consequently, the present method of predicting these loads is based on the application of nonplanar lifting surface theory to the foremost problem of wing-pylon interaction. The wing-pylon model is limited to incompressible flow and simple two-dimensional source theory has been used for thickness effects. The integral equations are solved numerically for a systematic series of wings with pylons of varying size at different spanwise and chordwise positions. The theory of Weber and Hawk for evaluating the mutual interference between tailplane-fin-fuselage arrangements in a constant sidewind is proposed for calculating store-pylon interference and slender body theory is used to determine the side forces on the nose and tail fins of the store. Estimated side forces and yawing moments are in satisfactory agreement with experimental results.

Nomenclature

$c(y)$	=	chord of wing at spanwise station y
$c(z)$	=	chord of pylon at spanwise station z
C_L	=	section lift coefficient
C_Y	=	side-force coefficient
C_n	=	yawing moment coefficient
C_P	=	chord of pylon
C_W	=	chord of wing in junction
$g_j^{(m)}(\eta_0)$	=	spanwise interpolation function
$h_i^{(n)}(\xi_0)$	=	chordwise interpolation function
$K_1(x,y)$	=	kernel function defined in Eq. (5)
$K_2(x,y)$	=	kernal function defined in Eq. (6)
$m_1m_2m_3$	=	number of spanwise loading (and velocity) points
$n_1n_2n_3$	=	number of chordwise loading (and velocity) points
$S_1S_2S_3$	=	span of left and right wing panels and pylon, respectively
x,y,z	=	rectangular Cartesian coordinates
$\bar{X}$	=	chordwise location of center of pressure of pylon side force
$x_L(y)$	=	coordinate of wing leading edge at spanwise station y
$x_L(z)$	=	coordinate of pylon leading edge at spanwise station z
X_P	=	chordwise location of pylon from wing leading edge
Y_P	=	spanwise location of pylon from wing centerline (fraction of semispan)
Z_P	=	depth or span of pylon
$\alpha(x_0,y_0)$	=	local slope of mean camber line (wing)
$\beta(x_0,z_0)$	=	local slope of mean camber line (pylon)
$\Delta C_P(x_0,y_0)$	=	wing lifting pressure coefficient
$\Delta C_P(x_0,z_0)$	=	pylon side force pressure coefficient

Reference area for C_Y is maximum store cross section unless otherwise stated. Reference length for C_n is maximum diameter. C_P, X_P, and Z_P are expressed as fractions of C_W.

Introduction

STORE separation disturbances contribute significantly to the total system error associated with the delivery of air-to-ground free-fall weapons. Unsatisfactory store separation may result also in serious store-to-aircraft collisions, particularly during high-speed dive bombing. It is now recognized that the general store separation problem has as its primary cause the large aerodynamic loads acting on the store in the captive position.

Several attempts have been made to estimate external store loads theoretically.[1] Most commonly, the problem has been approached by combining slender-body theory with the estimated flowfield induced by the wing-fuselage combination and by employing semiempirical or approximate analytical techniques to allow for the complex wing-pylon interaction problem.[2,3] The present method, on the other hand, is based on the premise that wing-pylon interference should be considered in more detail and is therefore structured around a more exact analytical model of the wing-pylon arrangement. Experiment adequately justifies this approach.

Recent advances in finite element and vortex lattice theory suggest alternative and more general approaches to the present problem.[4,5] The fact that external store loading calculations based on these more sophisticated methods do not yet seem to have appeared in the unclassified literature is surprising. In comparison with these methods, however, the present method is easy to apply and yields reasonable results with minimum computational effort. It thus constitutes a useful predesign tool.

The wing-pylon model is developed using incompressible nonplanar lifting surface theory in conjunction with simple two-dimensional source theory for the thickness effect and gives the distribution of aerodynamic side force

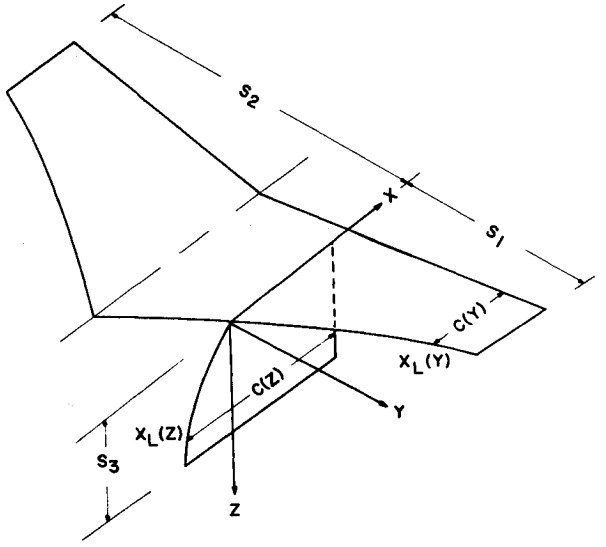

Fig. 1 Diagram of wing-pylon combination.

Presented as Paper 72-971 at the AIAA 2nd Atmospheric Flight Mechanics Conference, Palo Alto, Calif., September 11-13, 1972; submitted October 4, 1972; revision received October 30, 1973.

Index categories: Aircraft Aerodynamics (Including Component Aerodynamics); Aircraft Structural Dynamics.

*Research Scientist; presently Visiting Instructor, Naval Postgraduate School, Monterey, California.

on general pylon arrangements in combination with wings of arbitrary plan-form and camber. The method used for the expansion in series of the spanwise and chordwise loading functions is that given by Davies in his treatment of the oscillating T-tail.[6] Interference carryover loads between the pylon and the store are estimated using a constant sidewind theory of tailplane-fin-fuselage interaction.[7] Slender-body theory is used to evaluate the loads acting on the nose and tail-fins of the store due to local sidewash effects.

Wing-Pylon Analysis

The incompressible potential $\phi(x,y,z)$ for the very thin wing-pylon arrangement shown in Fig. 1 can be shown to be[8]

$$\phi(x,y,z) = \frac{V_\infty}{8\pi}\int_W\int \frac{\Delta C_P(x_0,y_0)}{(y-y_0)^2+z^2}z \left[1+\frac{x-x_0}{[(x-x_0)^2+(y-y_0)^2+z^2]^{1/2}}\right]dx_0dy_0 + \frac{V_\infty}{8\pi}\int_P\int \frac{\Delta C_P(x_0,z_0)}{(z-z_0)^2+y^2}y \left[1+\frac{x-x_0}{[(x-x_0)^2+y^2+(z-z_0)^2]^{1/2}}\right]dx_0dz_0 \quad (1)$$

where it is required to determine the pressure loading $\Delta C_P(x_0,y_0)$ on W and $\Delta C_P(x_0,z_0)$ on P. Equation (1) is differentiated first with respect to z (limit $z \to 0$) and then with respect to y (limit $y \to 0$) and the results equated respectively to the local surface slopes $\alpha(x,y)$ on W and $\beta(x,z)$ on P. This is the tangency condition. It is then convenient to introduce the new coordinates

$$\xi = \frac{x-x_L(y)}{c(y)} \qquad \epsilon = \frac{x-x_L(z)}{c(z)} \quad (2)$$

$$\eta = y/S_1 (y>0) \qquad \eta = y/S_2 (y<0), \qquad \zeta = z/S_3$$

where (Fig. 1) $c(y)$ and $x_L(y)$ denote the chord length and leading edge of the wing at $\eta = y/S_1 (y>0)$ or $\eta = y/S_2 (y<0)$ and $c(z)$ and $x_L(z)$ denote similar quantities at $\zeta = z/S_3$ on the pylon. The following pair of integral equations result:

$$\alpha(\xi,\eta) = \frac{S_1}{8\pi}\int_0^1 c(y_0)d\eta_0\int_0^1 \Delta C_P(\xi_0,\eta_0)K_1(x-x_0,y-y_0)d\xi_0 + \frac{S_2}{8\pi}\int_{-1}^0 c(y_0)d\eta_0\int_0^1 \Delta C_P(\xi_0,\eta_0)K_1(x-x_0,y-y_0)d\xi_0 + \frac{S_3}{8\pi}\int_0^1 c(z_0)d\zeta_0\int_0^1 \Delta C_P(\epsilon_0,\zeta_0)K_2(x-x_0,y,z_0)d\epsilon_0 \quad (3)$$

$$\beta(\epsilon,\zeta) = \frac{S_1}{8\pi}\int_0^1 c(y_0)d\eta_0\int_0^1 \Delta C_P(\xi_0,\eta_0)K_2(x-x_0,y_0,z)d\xi_0 + \frac{S_2}{8\pi}\int_{-1}^0 c(y_0)d\eta_0\int_0^1 \Delta C_P(\xi_0,\eta_0)K_2(x-x_0,y_0,z)d\xi_0 + \frac{S_3}{8\pi}\int_0^1 c(z_0)d\zeta_0\int_0^1 \Delta C_P(\epsilon_0,\zeta_0)K_1(x-x_0,z-z_0)d\epsilon_0 \quad (4)$$

$$K_1(x,y) = \frac{1}{y^2}\left[1+\frac{x}{(x^2+y^2)^{1/2}}\right] \quad (5)$$

$$K_2(x,y,z) = \frac{yz}{(y^2+z^2)^2}\left[2+\frac{2x^3+3x(y^2+z^2)}{(x^2+y^2+z^2)^{3/2}}\right] \quad (6)$$

The loading functions may be expressed analytically so that the coefficients in the series development of $\Delta C_p(\xi_0,\eta_0)$ and $\Delta C_p(\epsilon_0,\zeta_0)$ represent the unknown ΔC_p's at prescribed loading points which we denote (ξ_i,η_j) on W and (ϵ_i,ζ_j) on P. Loading discontinuities on the wing at the pylon junction must be allowed for, however, and this requires independent developments in series for $\eta > 0$ and $\eta < 0$. The integration is then performed numerically for a number of (ξ,η) and (ϵ,ζ) combinations equal to the number of loading points. Let us denote these combinations by (ξ_k,η_r) on W and by (ϵ_k,ζ_r) on P and refer to them as the velocity points. The resulting set of simultaneous algebraic equations is solved finally for the unknown pressure loading coefficients.

In the wing-pylon junction the leading and trailing edges of the pylon need not coincide with those of the wing. The chord lengths may also be different and the span of the wing is generally much greater than that of the pylon. For these reasons the size of the collocation mesh is allowed to be different for each panel. Accordingly, with n and m denoting the number of chordwise and spanwise points, respectively, we shall consider the mesh sizes $(n_1 \times m_1)$ for the left wing; $(n_2 \times m_2)$ for the right wing; and $(n_3 \times m_3)$ for the pylon. Following Davies, we assume for the loading on the left wing panel

$$\Delta C_P(\xi_0,\eta_0) = \sum_{i=1}^{n_1}\Delta C_P(\xi_i,\eta_0)h_i^{(n_1)}(\xi_0), \quad (\eta_0 = \text{const})$$
$$\Delta C_P(\xi_0,\eta_0) = \sum_{i=1}^{m_1}\Delta C_P(\xi_0,\eta_j)g_j^{(m_1)}(\eta_0), \quad (\xi_0 = \text{const}) \quad (7)$$

where the chordwise interpolation polynominal $h_i^{(n)}(\xi_0)$ is given in the Appendix as the product of $[(1-\xi_0)/\xi_0]^{1/2}$ with a polynominal of degree $(n-1)$; it is unity at $\xi_0 = \xi_i$ and zero at the remaining $(n-1)$ chordwise loading points. Similarly, $g_j^{(m)}(\eta_0)$ is the product of $(1-\eta_0)^{1/2}$ with a polynominal of degree $(m-1)$; it is unity at $\eta_0 = \eta_j$ and zero at the remaining $(m-1)$ spanwise loading points. The loading along a chord of the wing is thus seen to behave in the classical two-dimensional manner at the leading and trailing edges while along the span the behavior at the tips is that of the slender-wing theory. Expressions for the loading points (ξ_i,n_j) and the velocity points (ξ_k,η_r) are given in the Appendix.

Approaching the chordwise integration first, let us substitute the first of Eq. (7), together with similar expressions for the right wing and the pylon, into the integral Eqs. (3) and (4)

$$\alpha(\xi,\eta) = S_1\sum_{i=1}^{n_1}\int_0^1 \frac{\Delta C_P(\xi_i,\eta_0)}{(y-y_0)^2}I_i^{(n_1)}(\eta,\eta_0,\xi)d\eta_0 + S_2\sum_{i=1}^{n_2}\int_{-1}^0 \frac{\Delta C_P(\xi_i,\eta_0)}{(y-y_0)^2}I_i^{(n_2)}(\eta,\eta_0,\xi)d\eta_0 + S_3\sum_{i=1}^{n_3}\int_0^1 \frac{z_0\Delta C_P(\epsilon_i,\zeta_0)}{(y^2+z_0^2)^2}J_i^{(n_3)}(\eta,\zeta_0,\xi)d\zeta_0 \quad (8)$$

$$\beta(\epsilon,\zeta) = S_1\sum_{i=1}^{n_1}\int_0^1 \frac{y_0\Delta C_P(\xi_i,\eta_0)}{(y_0^2+z^2)^2}M_i^{(n_1)}(\zeta,\eta_0,\epsilon)d\eta_0 + S_2\sum_{i=1}^{n_2}\int_{-1}^0 \frac{y_0\Delta C_P(\xi_i,\eta_0)}{(y_0^2+z^2)^2}M_i^{(n_2)}(\zeta,\eta_0,\epsilon)d\eta_0 + S_3\sum_{i=1}^{n_3}\int_0^1 \frac{\Delta C_P(\epsilon_i,\zeta_0)}{(z-z_0)^2}N_i^{(n_3)}(\zeta,\zeta_0,\epsilon)d\zeta_0 \quad (9)$$

where

$$I_i^{(n)}(\eta,\eta_0,\xi) = \frac{c(y_0)}{8\pi}\int_0^1 h_i^{(n)}(\xi_0)\left[1 + \frac{x - x_0}{[(x-x_0)^2 + (y-y_0)^2]^{1/2}}\right]d\xi_0 \quad (10)$$

$$J_i^{(n)}(\eta,\zeta_0,\xi) = \frac{yc(z_0)}{8\pi}\int_0^1 h_i^{(n)}(\epsilon_0)\left[2 + \frac{2(x-x_0)^3 + 3(x-x_0)(y^2+z_0^2)}{[(x-x_0)^2 + y^2 + z_0^2]^{3/2}}\right]d\epsilon_0 \quad (11)$$

$$M_i^{(n)}(\zeta,\eta_0,\epsilon) = \frac{zc(y_0)}{8\pi}\int_0^1 h_i^{(n)}(\xi_0)\left[2 + \frac{2(x-x_0)^3 + 3(x-x_0)(y_0^2+z^2)}{[(x-x_0)^2 + y_0^2 + z^2]^{3/2}}\right]d\xi_0 \quad (12)$$

$$N_i^{(n)}(\zeta,\zeta_0,\epsilon) = \frac{c(z_0)}{8\pi}\int_0^1 h_i^{(n)}(\epsilon_0)\left[1 + \frac{x - x_0}{[(x-x_0)^2 + (z-z_0)^2]^{1/2}}\right]d\epsilon_0 \quad (13)$$

and where the $\int$ signs in Eqs. (8) and (9) denote evaluation using Manglers Principal Value Technique.[8] The first and second integrals, for example, possess nonintegrable singularities for $y > 0$ and $y < 0$, respectively.

Noting that an integration by parts prior to numerical integration removes the difficulty associated with the singular leading edge behavior of $h_i^{(n)}(u)$, which may be integrated explicitly, there are no further singularities to deal with in evaluating the influence coefficients and although the J and M integrals exhibit rapid variations near the wing-pylon junction the chordwise integration is now straightforward.

The remaining integration is performed using the spanwise interpolation function $g_j^{(m)}(\eta_0)$ to express the spanwise variation of the product terms $\Delta C_p(\xi_i,\eta_0)$-$I_i^{(n_1)}(\eta,\eta_0,\xi)$ etc., which appear in Eqs. (8) and (9). Accordingly, when equations of the form

$$\Delta C_p(\xi_i,\eta_0)I_i^{(n_1)}(\eta,\eta_0,\xi) = \sum_{j=1}^{m_1}\Delta C_p(\xi_i,\eta_j)I_i^{(n_1)}(\eta,\eta_j,\xi)g_j^{(m_1)}(\eta_0) \quad (14)$$

for integration over the left wing panel (η_0 and $\eta_j > 0$; $-1 \le \eta \le 1$) and

$$\Delta C_p(\xi_i,\eta_0)I_i^{(n_2)}(\eta,\eta_0,\zeta) = \sum_{j=m_1+1}^{m_1+m_2}\Delta C_p(\xi_i,\eta_j)I_i^{(n_2)}(\eta,\eta_j,\xi)g_j^{(m_2)}(\eta_0) \quad (15)$$

for integration over the right wing panel (η_0 and $\eta_j < 0$; $-1 \le \eta \le 1$) are substituted into the integral equations and when $\alpha(\xi,\eta)$ and $\beta(\epsilon,\zeta)$ are replaced by their values $\alpha(\xi_k,\eta_r)$ and $\beta(\epsilon_k,\zeta_r)$ at the velocity points the following simultaneous algebraic equations result

$$\alpha(\xi_k,\eta_r) = S_1\sum_{j=1}^{m_1}\sum_{i=1}^{n_1}\Delta C_p(\xi_i,\eta_j)I_i^{(n_1)}(\eta_r,\eta_j,\xi_k)\int_0^1 \frac{g_j^{(m_1)}(\eta_0)}{(y_r-y_0)^2}d\eta_0 + S_2\sum_{j=m_1+1}^{m_1+m_2}\sum_{i=1}^{n_2}\Delta C_p(\xi_i,\eta_j)I_i^{(n_2)}(\eta_r,\eta_j,\xi_k)\int_{-1}^0 \frac{g_j^{(m_2)}(\eta_0)}{(y_r-y_0)^2}d\eta_0 + S_3\sum_{j=1}^{m_3}\sum_{i=1}^{n_3}\Delta C_p(\epsilon_i,\zeta_j)J_i^{(n_3)}(\eta_r,\zeta_j,\xi_k)\int_0^1 \frac{z_0 g_j^{(m_3)}(\eta_0)}{(y_r^2+z_0^2)^2}d\zeta_0 \quad (16)$$

$$\beta(\epsilon_k,\zeta_r) = S_1\sum_{j=1}^{m_1}\sum_{i=1}^{n_1}\Delta C_p(\xi_i,\eta_j)M_i^{(n_1)}(\zeta_r,\eta_j,\epsilon_k)\int_0^1 \frac{y_0 g_j^{(m_1)}(\eta_0)}{(z_r^2+y_0^2)^2}d\eta_0 + S_2\sum_{j=m_1+1}^{m_1+m_2}\sum_{i=1}^{n_2}\Delta C_p(\xi_i,\eta_j)M_i^{(n_1)}(\zeta_r,\eta_j,\epsilon_k)\int_{-1}^0 \frac{y_0 g_j^{(m_2)}(\eta_0)}{(z_r^2+y_0^2)^2}d\eta_0 + S_3\sum_{j=1}^{m_3}\sum_{i=1}^{n_3}\Delta C_p(\epsilon_i,\zeta_j)N_i^{(n_3)}(\zeta_r,\zeta_j,\epsilon_k)\int_0^1 \frac{g_j^{(m_3)}(\zeta_0)}{(z_r-z_0)^2}d\zeta \quad (17)$$

Left Wing ($\eta > 0$) Right Wing ($\eta < 0$)

$k = 1,2,\cdots n_1$ $\quad k = 1,2,\cdots n_2$

$r = 1,2,\cdots m_1$ $\quad r = (m_1+1),(m_1+2),\cdots(m_1+m_2)$

$k = 1,2,\cdots n_3$ Pylon

$r = 1,2,\cdots m_3$

With regard to the thickness problem the horizontal perturbation velocity $u(x,z)$ for a moderately thick symmetric two-dimensional aerofoil at zero incidence in incompressible flow is

$$u(x,z) = \frac{V_\infty}{\pi}\int_0^c \frac{(x-x_0)dZ/dx_0}{(x-x_0)^2+z^2}dx_0 \quad (18)$$

where x is measured from the leading edge and Z is the profile. Employing simple sweep theory the lateral perturbation velocity $v(x,z)$ for a sheared wing with leading edge sweep Λ follows from Eq. (18) as

$$v(x,z) = -\frac{V_\infty \cos^2\Lambda \sin\Lambda}{\pi}\int_0^c \frac{(x-x_0)dZ/dx_0}{(x-x_0)^2\cos^2\Lambda + z^2}dx_0 \quad (19)$$

where the sign denotes the inboard sense of the sidewash.

Using this result the lifting wing-pylon combination of finite thickness can be replaced by one of zero thickness provided the tangency condition on the pylon associated with the influence of wing thickness and sweep is first satisfied at the velocity points (ϵ_k,ζ_r) by introducing the camber $\beta(\epsilon_k,\zeta_r) = v(\epsilon_k,\zeta_r)/V_\infty$.

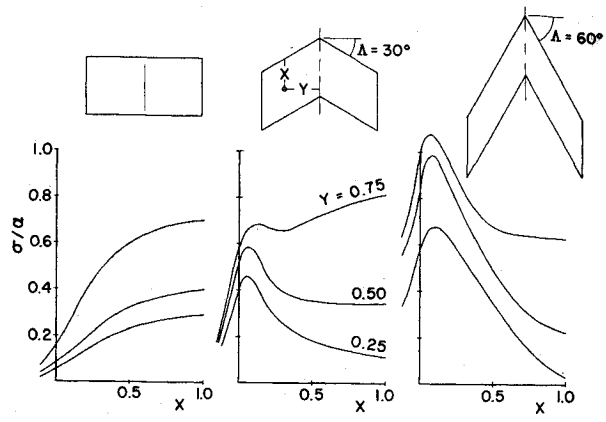

Fig. 2 Sidewash characteristics at 0.2 wing chords below untapered wings with $A = 2$

Wing-Pylon Sideload Characteristics

The integral equations have been solved numerically for a systematic series of geometrical arrangements with different wing sweepback angles, pylon spanwise and chordwise locations, pylon chord lengths, and pylon depths. Of basic interest here is the sidewash angle induced below a particular family of untapered wings of aspect ratio 2 at three spanwise positions. These results are shown in Fig. 2 and were obtained by solving Eq. (16) for the wing alone. The subsequent loading was substituted in Eq. (1) which

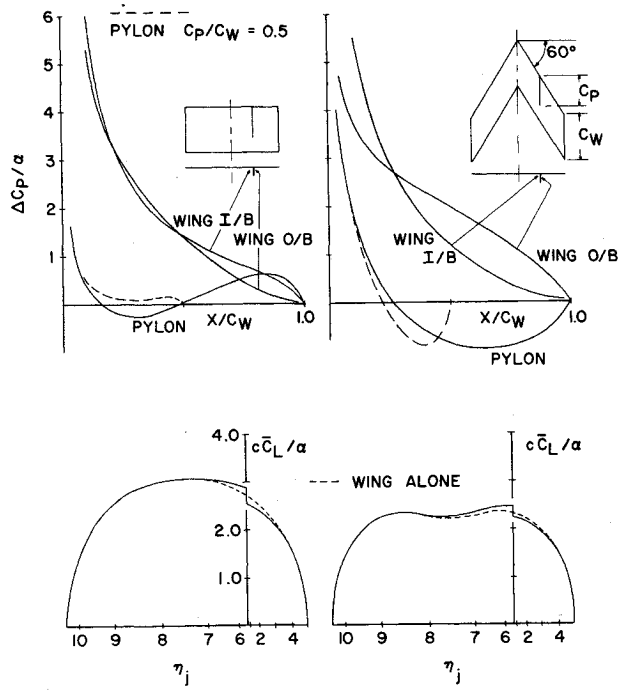

Fig. 3 Pressure coefficient in wing-pylon junction and spanwise wing loading for untapered wings with $A = 2$.

was then differentiated with respect to y. Entirely different lateral flow fields exist below the rectangular and highly swept wings.[9] The consequence of this in terms of the present nonplanar interaction problem is discussed below.

Figure 3 shows the spanwise wing loading and the distribution of junction lift and side force for the rectangular and 60° swept wings in combination with rectangular pylons. In the cases where the pylon chord (C_P) and the wing chord (C_W) are equal, three (3) chordwise and five (5) spanwise collocation point stations were used for each wing panel and for the pylon. With $C_P = C_W/2$, five (5) chordwise points were used on the wing to adequately converge the solution.

In the wing alone cases the spanwise loading curves are in good agreement with those obtained using other methods. It should be noted that they have been obtained, however, with a disposition of spanwise collocation points which is entirely asymmetric with respect to the wing centerline.

The presence of the pylon (depth $Z_P = 0.2\ C_W$) is seen to result in a strong local discontinuity in wing lift which behaves like $x^{-1/4}$ close to the leading edge in the outboard junction and like $x^{-3/4}$ close to the leading edge in the inboard junction. Clearly, the pylon acts as an effective vertical reflection plane, bringing about a redistribution of lift along the chord similar to that found in the center ($x^{-1/4}$) and close to the tips ($x^{-3/4}$) of isolated swept wings.[10] As a consequence of this, in addition to the discontinuity in lift, the chordwise position of the local aerodynamic center may be considerably closer to the wing leading edge on the inboard side of the pylon than on the outboard side.

The pressures on the upper wing surface must be continuous along the junction and consequently the nonplanar theory should predict for the local side-force pressure coefficient along the junction chord the difference between the corresponding inboard and outboard lifting pressure coefficients. This is indeed the case in Fig. 3 for the swept wing. For the rectangular wing, however, the agreement is qualitatively correct only. However, it should be pointed out that the double curvature of the side-force distribution in the junction provides here an extreme test case for the theoretical method, which makes no attempt to introduce a condition of pressure balance along the junction chord. Further, this predicted curvature seems entirely reasonable in view of Fig. 2 which shows a steady increase in lateral flow velocity with increasing distance behind the leading edge (the reverse is true for the swept wing). As a final note on the theoretical prediction of pressures in the junction, results for the smaller pylon ($C_P/C_W = 0.5$) may be mentioned. Thus, while the calculated wing ΔC_P's behind the pylon trailing edge were in close agreement for points immediately to the left and right of the pylon station, they were not exactly equal. On the other hand, the integrated pressure balance along the junction chord was entirely satisfactory.

In the case of the 60° swept wing a strong reversal occurs in the outboard sense of the junction side loading at about 25% chord. Notwithstanding the much larger average lateral flow velocities which occur below this wing (Fig. 2), this suggests that total integrated pylon side forces could be smaller below wings with high sweepback angles. On the other hand, pylon side moments below

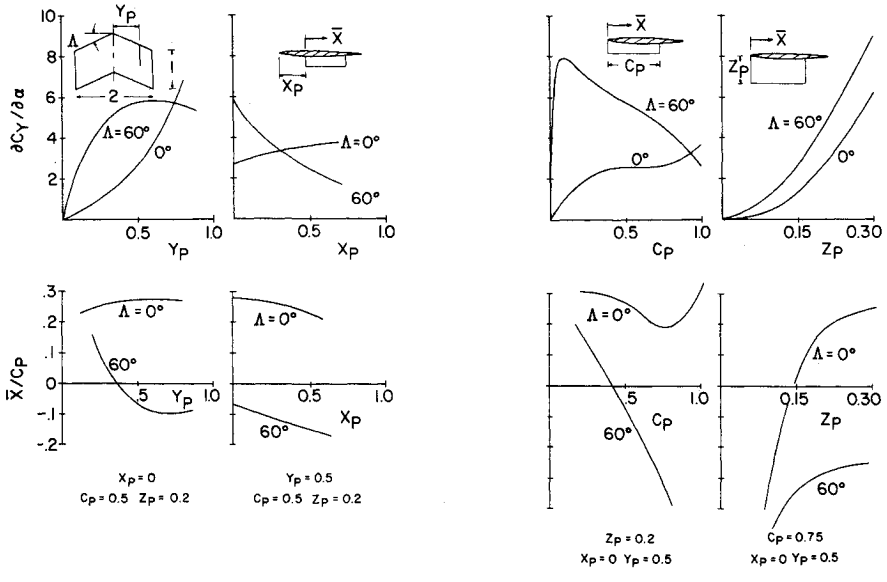

Fig. 4 Pylon side-force coefficient and chordwise center of pressure for different wing-pylon arrangements at angle-of-attack.

highly-swept wings could be considerable. The results shown in Fig. 3 suggest also that the total pylon side force may increase as the pylon chord is reduced.

The total side force coefficient derivative $\partial C_Y/\partial\alpha$† and the chordwise center of pressure position $\bar{X}$ for a variety of pylon arrangements in combination with zero-thickness rectangular and 60° sweptback wings are given in Fig. 4. These results may be interpreted conveniently on the basis of the preceding discussion. For example, pylons located outboard of 75% wing semispan may indeed experience larger side forces below rectangular wings. This is also the case at 50% wing semispan when the pylon leading edge is moved towards the wing trailing edge. Furthermore, for the swept-wing combination, $\partial C_Y/\partial\alpha$ decreases with increasing pylon chord length in such a manner that the total pylon side force remains practically constant. The center of pressure, however, moves to large distances forward of the pylon leading edge.

Limiting Cases

Two interesting limiting cases arise in the study of wing-pylon interaction. Consider first the accuracy with which a pure sideslip or β induced side-force may be estimated by assuming the wing to act as a perfect horizontal reflection plane. Figure 5 (upper) shows the exact distribution of pylon side-force (nonplanar model) for a rectangular wing of aspect ratio 2 in combination with rectangular pylons of various depth Z_P. Also shown are the corresponding results for an isolated rectangular *wing* of aspect ratio $2Z_P$ at *incidence* β. Jones' theory for total side force as $Z_P \to 0$ is also indicated.[11] For $Z_P < 0.4$, side force and side-force distribution are in perfect agreement using the two methods; for $Z_P = 3.0$ the error is about 10%.

For the same arrangement, Fig. 5 (lower) shows side force due to incidence. As noted earlier, the double curvature of the $\Delta C_P/\alpha$ curve along the junction chord (for $Z_P = 0.2$) is apparently caused by a strong chordwise gradient in wing-induced sidewash. This is most pronounced close to the wing surface. In the case $Z_P = 0.4$ the junction pressure distribution changes in a manner which suggests the influence of a more uniform sidewash field. The limiting $\Delta C_P/\alpha$ curve in the junction occurs for $Z_P = 3$ (wing chords) and may be estimated crudely if we replace the pylon by a perfect vertical reflection plane. The side-force pressure coefficient then becomes one-half the difference between the lifting pressure coefficients estimated along the centerlines of two isolated wings with half-span geometries identical to those of the given outboard and inboard wing panels. This result agrees, at least qualitatively, with the nonplanar theory. The pylon span loading curves in this case are of particular interest; they are approximately elliptical for small Z_P and concave for $Z_P > 3$.

Store Interference

An incompressible flow theory is developed in Ref. 7 for calculating the side force on fuselage-fin-tailplane arrangements in a sidewind. If the tailplane span is allowed to become large these results may be used to estimate the mutual interference between the body of the store and the pylon in the present problem. Accordingly, in Fig. 6, the basic pylon side force $P(0)$ is to be calculated using the wing-pylon analysis outlined previously. $P(S)$ and $S(P)$ are then the side forces acting on the pylon in the presence of the store and on the store in the presence of the pylon, respectively. $S(P)$ is a pylon carry-over load and

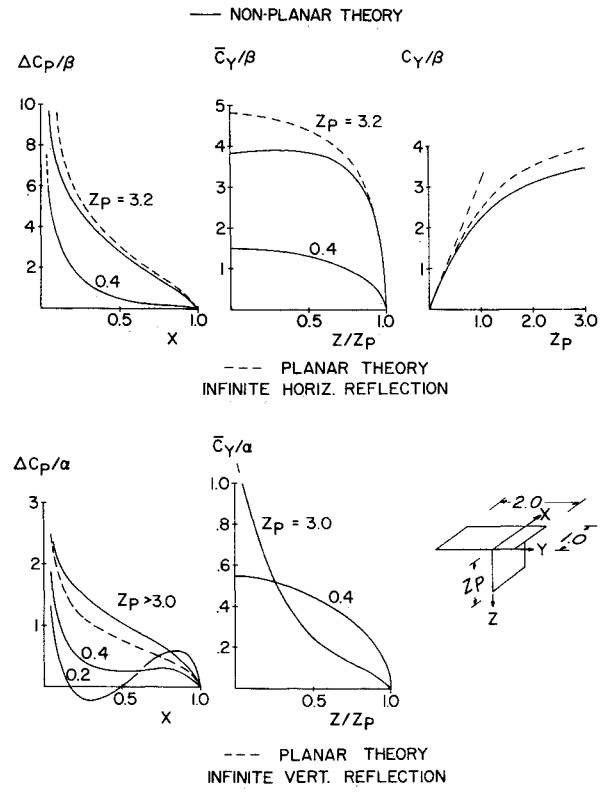

Fig. 5 Limiting pylon sideload distributions.

does not include wing-induced sidewash loads on the nose and tail of the store.

The constant sidewind is inconsistent with the fact that the pylon is generally located in extremely nonuniform flow; an exception being the case of a very thin wing-pylon combination in pure sideslip. Furthermore, when the radius of the main body of the store varies, it is necessary to use the average value of R/Z_P along the store-pylon junction. Finally, in order to evaluate the interference yawing moment on the store, the same chordwise center-of-pressure location is to be assumed for the $S(P)$ carry-over load as that determined for the basic $P(0)$ load.

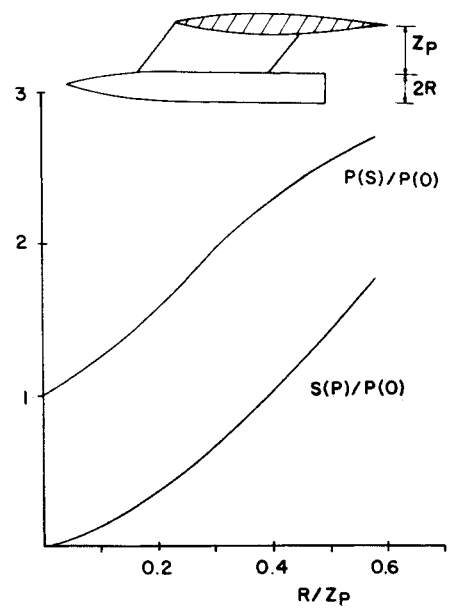

Fig. 6 Variation of interference sideloads with ratio of store radius to pylon depth.

†C_Y is referenced to pylon area.

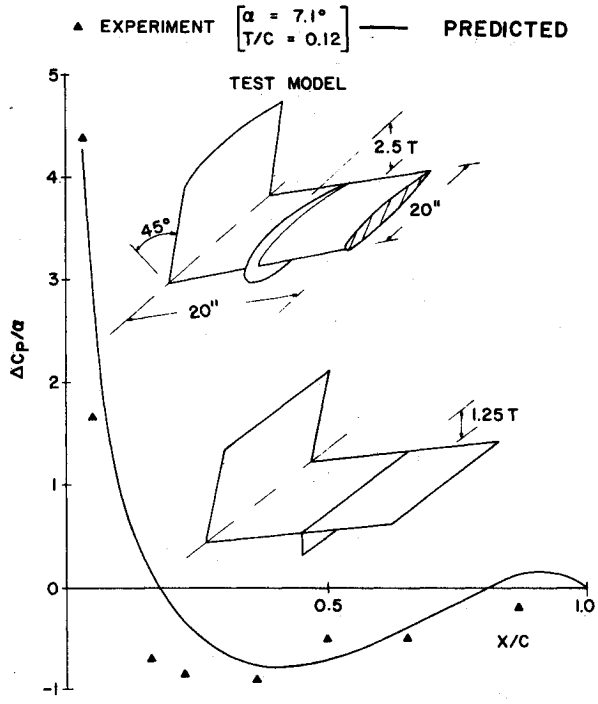

Fig. 7 Side-force pressure coefficient in junction of 45° swept wing-fence combination.

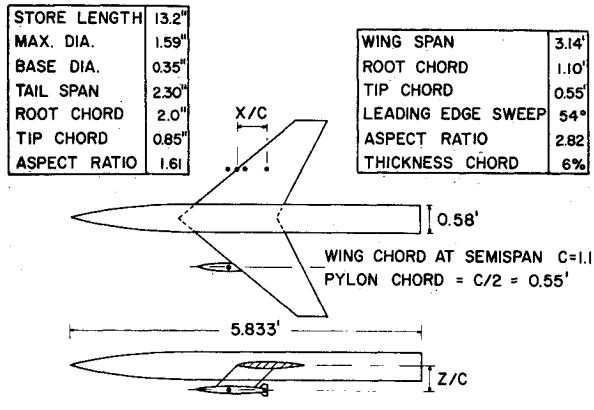

Fig. 8 The ARA model geometry.

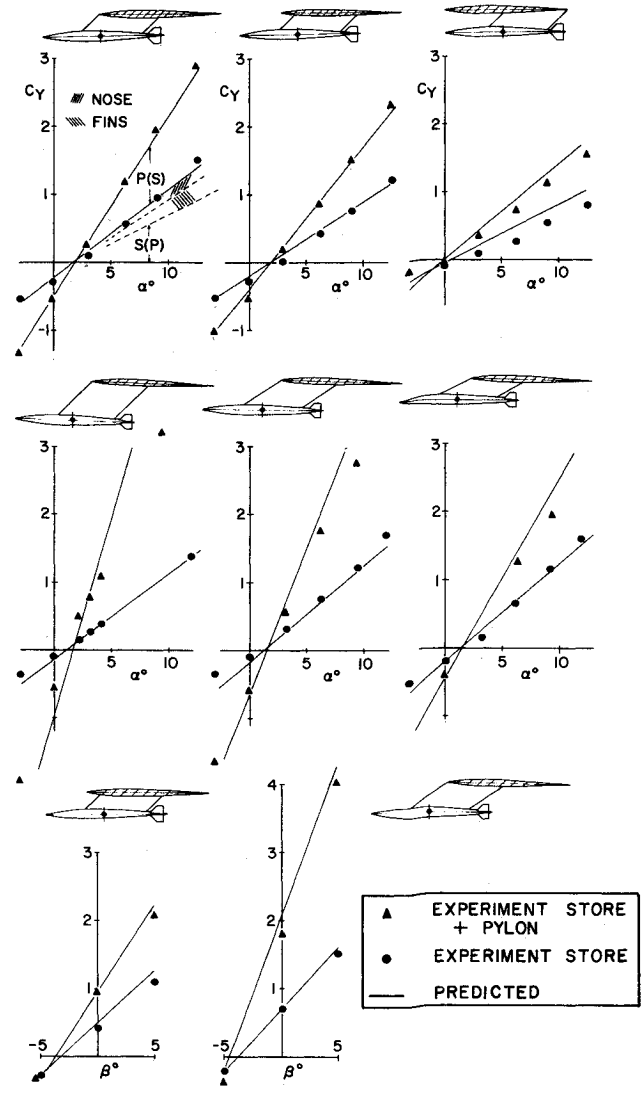

Fig. 9 Comparison with experimental side-force measurements.

Evidently, the above procedure oversimplifies the true wing-pylon-store interaction problem. Nevertheless, by avoiding the more complex and expensive methods mentioned earlier, it was hoped that the approximations would prove reasonable for predesign purposes. Figure 6 is therefore to be used as the basis for all store-pylon interference calculations.

Comparison with Experiment

There is a surprising absence of generally available pressure measurements on wing-pylon combinations and only the experimental data presented in Fig. 7, showing the side-force pressure coefficient in the junction of a 12% thick, 45° swept wing-fence combination, could be found.[12] These tests were conducted at 200 fps at α = 7.1° and in Fig. 7 the effects of thickness have been removed from the test data. Notwithstanding the fence on the upper wing surface, the large leading-edge fence radius, and the thick wing section, these data tend nevertheless to confirm the predicted reversal in local side force behind the leading-edge.

The over-all prediction method has been tested by comparing integrated forces and moments with the results of a series of wind-tunnel tests conducted by the Aeronautical Research Association in England.[13,14] Figure 8 gives geometric data on the test model. The swept-forward pylons have a constant chord, equal in length to one-half the local wing chord, and were positioned at wing semispan where fuselage interference effects are small.[9] Side forces and yawing moments were measured with the fins-on (and in some cases with fins-off) on the store and on the combined store-pylon assembly.

In Fig. 9 measured side force is shown against incidence (sideslip β = 0) and against sideslip (incidence α = 6°) for several of the ARA store-pylon arrangements. The first set of results are for pylons of constant depth (Z/C_W = 0.17) and for three chordwise positions of the store center-of-gravity (X/C_W = 0, 0.15, and 0.5). Here Z and X were measured from the wing chord plane to the store center

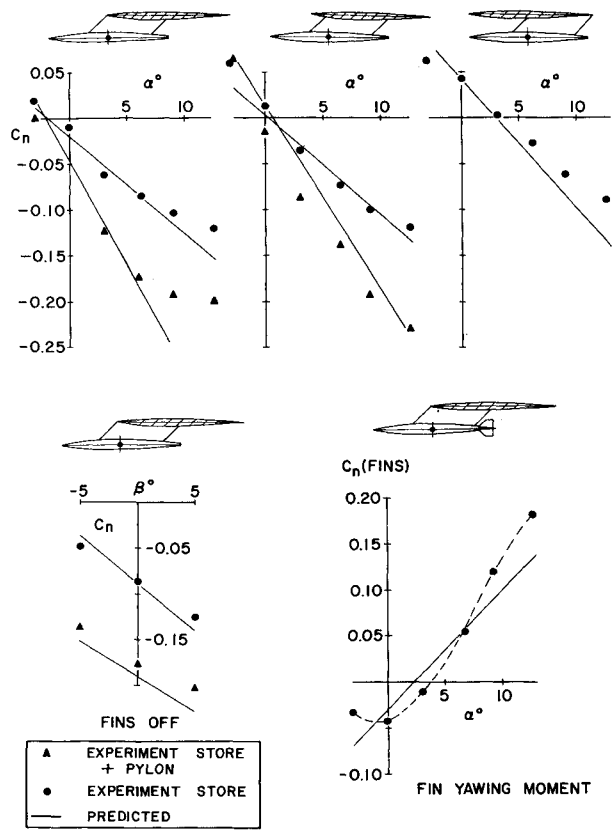

Fig. 10 Comparison with experimental yawing moment measurements.

line and from the wing leading edge, respectively. The second set of results are for $X/C_W = -0.15$ with $Z/C_W = 0.35$, 0.26, and 0.17, respectively.

Agreement with the theory is entirely satisfactory except for the case in which the pylon and wing trailing edges coincide. In this case it should nevertheless be noted that the theory is successful in predicting a significant decrease in side force as the pylon is moved rearwards (see also Fig. 4). The theoretical breakdown of side force further indicates that the pylon carry-over load may represent as much as 60% of the total load on the store. As a final observation in Fig. 9 it is interesting to translate the highest measured coefficient ($C_Y = 4.0$ for $\alpha = 6°$ and $\beta = 5°$) into pounds of side force for a practical situation: In the case of an aircraft with 10-times the ARA model scale flying at 0.8 M at sea level this amounts to 5500 lb.

The potential flow model was unable to predict accurately the yawing moment associated with the small tail fins. For this reason in Fig. 10 yawing moment is shown against α and β fins-off and the contribution due to the tail fins is shown separately. The yawing moment at zero incidence is worth noting, particularly for the most rearward pylon location. In this case C_{y0} was approximately zero and therefore C_{n0} is the result of an almost pure aerodynamic couple.

The inability of the linear theory to predict the fin yawing moment is evident from Fig. 10. The fin side force, however, was generally predicted to within 10%. Compared with the fins-off case, this indicates that the extremely close proximity of the fins to the pylon may be causing a significant redistribution of store-pylon pressure. Furthermore, the tail fins are located in the pylon wake and in the core of a trailing circulation vortex which emanates from the store. As the angle of attack increases through about 2° the pylon loading and therefore the sense of the circulation around the store change sign. These are given as possible explanations for the nonlinear tail-fin behavior shown in Fig. 10.

Conclusions

A method for calculating the side loads on external-stores at low subsonic speeds has been described. The method deals with the complex wing-pylon-store interaction problem by first determining the loads on the pylon in combination with the wing. Interference carry-over loads between the pylon and the store are subsequently evaluated using a constant sidewind theory of tailplane-fin-fuselage interaction.

The aerodynamic loading on a systematic series of wing-pylon arrangements has been calculated and it is shown that the side force may vary in a totally unexpected manner with changes in wing sweep, pylon geometry, and pylon location. With care, however, these results may be used to give an indication of side loading for a range of practical situations. Additionally, some limiting nonplanar solutions have been compared with the results of plane wing theory for cases in which the pylon span is either very large or very small.

Predicted side forces and yawing moments for several wing-pylon-store arrangements exhibit satisfactory agreement with experiment.

Appendix: The Interpolation Functions

The interpolation functions $h_i^{(n)}(\xi_0)$ and $g_j^{(m)}(\eta_0)$ are required together with the loading points (ξ_i,η_j) and the velocity points (ξ_k,η_r). These are taken from Ref. (6) where an explanation of their derivation is given. The chordwise interpolation function is

$$h_i^{(n)}(\xi_0) = \frac{l_n(\xi_0)}{(\xi_0 - \xi_i)\left[\frac{d}{d\xi_0} l_n(\xi_0)\right]_{\xi_i}} \left(\frac{\xi_i}{1-\xi_i}\right)^{1/2} \left(\frac{1-\xi_0}{\xi_0}\right)^{1/2} \tag{A1}$$

where $l_n(\xi_0)$ is the orthogonal polynomial of degree n with the roots

$$\xi_i = \frac{1}{2} - \frac{1}{2}\cos\left(\frac{2i-1}{2n+1}\pi\right), \quad i = 1,2,\cdots,n \tag{A2}$$

and where

$$\xi_k = 1 - \xi_i \qquad k = 1,2,\cdots n \qquad i = n-k+1 \tag{A3}$$

Similarly, the spanwise interpolation function is

$$g_j^{(m)}(\eta_0) = \frac{\mu_m(\eta_0)(1-|\eta_0|)^{1/2}}{|\eta_0| - |\eta_j|\left[\frac{d}{d\eta_0}\mu_m(\eta_0)\right]_{\eta_j}(1-|\eta_j|)^{1/2}} \tag{A4}$$

where $\mu_m(\eta_0)$ is the Jacobi Polynomial

$$\mu_m(\eta_0) = \sum_{p=0}^{m} \frac{(-1)^p}{2^{2p}}\left(\frac{m!}{p!}\right)^2 \frac{(2m+2p+1)!\,|\eta_0|^p}{(m-p)!(m+p)!(2m+1)!} \tag{A5}$$

The loading and velocity points coincide in the spanwise sense and are the m_1 positive roots of the polynomial equation $\mu(m_1)(\eta_0) = 0$ for the port wing ($\eta > 0$) and the m_2 negative roots of $-\mu(m_2)(\eta_0) = 0$ for the starboard wing ($\eta < 0$).

References

[1]Marsden, P. and Haines, A. B., "Aerodynamic Loads on External Stores: A Review of Experimental Data and Methods of Prediction," R and M 3503, Nov. 1962, Aeronautical Research Council, London.

[2]Sadler, R. M., "External Stores Separation Under Subsonic Conditions," Memo 331, April 1961, Aerial Measurements Laboratory, Northwestern University, Ill.

[3]Bobbitt, P. J., et. al., "Calculation of External-Store Loads and Correlation With Experiment," NACA RM L57D30A, July 1957, NACA.

[4]Bradley, R. G. and Miller, B. D., "Application of Finite Element Theory to Airplane Configurations," *Journal of Aircraft,* Vol. 8, No. 6, June 1971, pp. 400–405.

[5]Kalman, T. P., Rodden, W. P., and Giesing, J. P., "Application of the Doublet-Lattic Method to Nonplanar Configurations in Subsonic Flow," *Journal of Aircraft,* Vol. 8, No. 6, June 1971, pp. 406–413.

[6]Davies, D. E., "Generalized Aerodynamic Forces on a T-Tail Oscillating Harmonically in Subsonic Flow," R and M 3422, May 1964, Aeronautical Research Council, London.

[7]Weber, J. and Hawk, A. C., "Theoretical Load Distributions on Fin-Body Tail-plane Arrangements in a Sidewind," RAE Rept. Aero. 2518, Aug. 1954, Royal Aircraft Establishment, England.

[8]Ashley, H. and Landahl, M., *Aerodynamics of Wings and Bodies,* Addison-Wesley, Reading, Mass.,1965, pp. 208–226.

[9]Alford, W. J., "Theoretical and Experimental Investigation of the Subsonic-Flow Fields Beneath Swept and Unswept Wings," NACA Rept. 1327, 1957, NACA.

[10]Kuchemann, D., "A Simple Method of Calculating the Span and Chordwise Loading on Straight and Swept Wings of Any Given Aspect Ratio at Subsonic Speeds," RAE Rept. Aero. 2476, Aug. 1952, Royal Aircraft Establishment, England.

[11]Jones, R. T., "Properties of Low-Aspect-Ratio Pointed Wings at Speeds Below and Above the Speed of Sound," NACA Rept. 835, 1946, NACA.

[12]Weber, J. and Lawford, J. A., "The Reflection Effect of Fences at Low Speeds," R and M 2977, May 1954, Aeronautical Research Council, London.

[13]Marsden, P. and Haines, A. B., "Measurements at Transonic Speeds of the Side Force and Yawing Moment on Various Store Arrangements Mounted Beneath a 45° Swept-Wing Fuselage Model," C.P. 955, June 1964, Aeronautical Research Council, London.

[14]Marsden, P., "Measurements of Store and Store/Pylon Loads at Transonic Speeds for Further Store Arrangements Mounted Beneath a 45° Swept-Wing Fuselage Model," ARA Model Test Note M10/1, May 1965, Aeronautical Research Association, Bedford, England.